IEEE Photonics Journal
An IEEE Photonics Society Publication

Open Access

# Multiple Plasmon-Induced Transparency Responses in a Subwavelength Inclined Ring Resonators System

Volume 7, Number 6, December 2015

**Kunhua Wen**
**Yihua Hu**
**Li Chen**
**Jinyun Zhou**
**Miao He**
**Liang Lei**
**Ziming Meng**

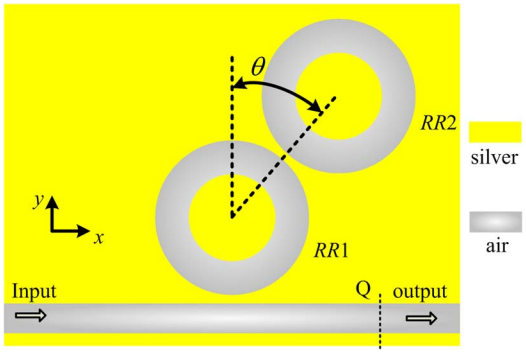


DOI: 10.1109/JPHOT.2015.2504966
1943-0655 © 2015 IEEE

IEEE photonics SOCIETY

IEEE

# Multiple Plasmon-Induced Transparency Responses in a Subwavelength Inclined Ring Resonators System

**Kunhua Wen, Yihua Hu, Li Chen, Jinyun Zhou, Miao He, Liang Lei, and Ziming Meng**

School of Physics and Optoelectronic Engineering, Guangdong University of Technology, Guangzhou 510006, China

*DOI: 10.1109/JPHOT.2015.2504966*


Manuscript received October 28, 2015; revised November 25, 2015; accepted November 27, 2015. Date of publication December 2, 2015; date of current version December 11, 2015. This work was supported in part by the National Natural Science Foundation of China under Grant 61405039 and Grant 61475037, by the Natural Science Foundation of Guangdong Province of China under Grant 2014A030310300, by the National High Technology Research and Development Programs of China under Grant 2013AA03A101, by the State Key Lab of Optical Technologies on Nano-Fabrication and Micro-Engineering of China, by the Foundation for Distinguished Young Talents in Higher Education of Guangdong under Grant 2014KQNCX066, and by the Research Fund of Guangdong University of Technology under Grant 13ZK0387. Corresponding author: K. Wen (e-mail: khwen@gdut.edu.cn).

**Abstract:** On the basis of single metal–insulator–metal (MIM) ring resonator (RR) structure, which acts as a band-stopped filter, a dual RR (DRR) system is proposed to obtain the plasmon-induced transparency (PIT) effect. By rotating the second RR an angle, double PIT windows are achieved due to the dual interference effects, which are attributed to different excitation pathways from the first RR to the second RR. In addition, triple PIT peaks are also achieved by adding an extra inclined RR to the DRR system. Phase shifts, which will occur at each transparency window, are also achieved and analyzed. These compact MIM waveguide structures may be used in the highly integrated optical circuits for biochemical sensors optical signal processing, and optical data storage.

**Index Terms:** Metal–insulator–metal (MIM), ring resonator (RR), plasmon-induced transparency (PIT).

## 1. Introduction

According to the quantum interference in multi-level atomic systems, electromagnetically induced transparency (EIT), which shows great potential applications for optical data storage and biosensor, is first found and demonstrated in the atomic media [1], [2]. However, the realization of the atomic EIT requires strict conditions, which quite limit its development and practical applications. Therefore, great efforts are made in the classical systems for realizing the EIT-like effect, such as the metamaterial-induced transparency [3], [4], phase-coupled plasmon-induced transparency [5], coupled dielectric resonators [6], [7], and so on. It is worth pointing out that plasmonic induced transparency (PIT) effects are also widely studied in the subwavelength structures, since surface plasmon polaritons (SPPs) trapped on the metal/insulator interface can break the classical diffraction limit and manipulate light in the nanoscale domain [8]–[10]. Among those plasmonic systems, metal-insulator-metal (MIM) waveguide structures have attracted considerable attention due to the advantages of deep subwavelength confinement of light, which is preferred in the

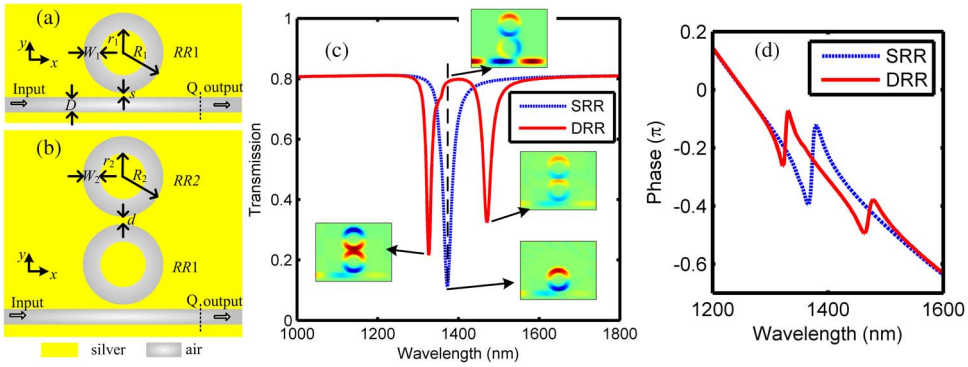


Fig. 1. (a) MIM waveguide SRR system, (b) MIM waveguide DRR system, (c) transmission spectra of the SRR and DRR systems, and (d) phase shift of the DRR system.

integrated photonics area [11]–[17]. Because they benefit from promising fabrication technologies, such as the lithography method, the focused ion beam (FIB) method, and the etching and template method [18]–[22], increasingly more MIM waveguide structures are explored to obtain the analog of EIT effects. For example, PIT phenomena were theoretically predicted and experimentally demonstrated by adding single or multiple grooves on the opposite sides or the same side of a MIM waveguide [23]–[27]. Besides, the transparency window was also observed in the side-coupled MIM detuned Fabry-Perot (FP) resonators [28]–[32], which could be a pair of cavities or single T-shaped resonator. However, there has been much research on the multi-level EIT effects, which will lead to multiple transparency peaks.

In this paper, we investigate the multi-level PIT transmission based on a compact side-coupled ring resonators (RRs) system. Dual vertical RRs are employed to obtain a transparency window which arises at the former forbidden band of the single RR structure. By rotating the dual RRs (DRRs) a certain angle, dual-peaks PIT response is obtained, since a new transmission peak will arise at a trough of the previous transparency window. Moreover, third order PIT transmission is obtained by using the triple RRs (TRRs) system. In addition to the two transmission peaks, the third peak is achieved at the other trough of the transparency window. The single, dual, and triple PIT windows in the plasmonic waveguide system are investigated by using the finite difference time domain method (FDTD) method. Therefore, this work may provide the way for the realization of nanoscale optical devices.

## 2. Analysis and Results

Usually, band-stopped spectrum can be obtained through a side-coupled-cavity MIM waveguide system, as shown in Fig. 1(a), where the metal and insulator are silver and air, respectively. For those MIM waveguide structures, the effective refractive index $n_{\text{eff}}$ can be obtained from the dispersion equation of TM mode and given by [33]

$$\varepsilon_i k_m + \varepsilon_m k_i \tanh(-jk_i d/2) = 0 \quad (1)$$

$$k_0 n_{\text{eff}} = \beta \quad (2)$$

where $k_0 = 2\pi/\lambda$ and $\beta$ are the wave number of light in the air and the waveguide, respectively, $k_{i,m} = \sqrt{\varepsilon_{i,m} k_0^2 - \beta^2}$ is the transverse propagation constants in the air and the silver, respectively, $d$ is the width of the waveguide, and $\varepsilon_i$ and $\varepsilon_m$ are the dielectric constants of air and silver, respectively. The real part $\text{Re}(n_{\text{eff}})$ and imaginary part $\text{Im}(n_{\text{eff}})$ of $n_{\text{eff}}$ determine the optical phase retardation and SPP propagation loss, respectively. Considering the structure in nano scale, we ignore $\text{Im}(n_{\text{eff}})$ and pay more attention to $\text{Re}(n_{\text{eff}})$ for controlling the resonance effects in the structure.

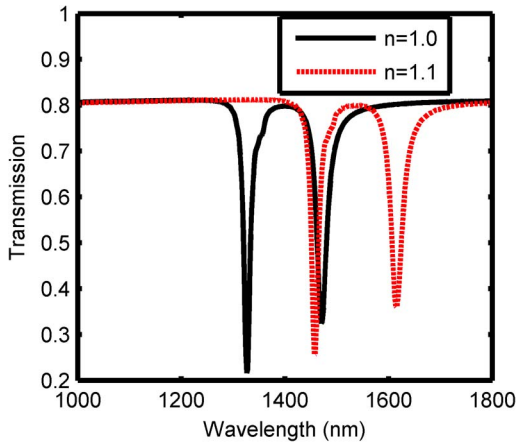


Fig. 2. Transmission spectra of DRR system with $n = 1.0$ and $n = 1.1$.

Usually, the ring cavity can perform as a FP resonator, and thus, a forbidden band will be achieved. FDTD method is used to investigate its performance. By defining the coupling distance as $s = 15$ nm, the width of the MIM bus waveguide as $D = 50$ nm, and the width, inner radius, and outer radius of the RR1 as $W_1 = 50$ nm, $r_1 = 130$ nm, and $R_1 = 130$ nm, respectively, a transmission trough at the wavelength of 1373 nm is achieved in this single RR (SRR) structure, as shown in Fig. 1(c) with blue dotted line. By adding another RR2 above the RR1 with a coupling distance of $d = 5$ nm, destructive interference of the two resonant modes in RR1 and RR2 will arise in this DRR system, as shown in Fig. 1(b). When the inner radius and outer radius of the RR2 are defined as $r_2 = 130$ nm, and $R_2 = 130$ nm, respectively, and other parameters keep no change, we can obtain the PIT transmission spectrum in Fig. 1(c) with red solid line. A transmission peak with a transmittance of ~0.8 is achieved at the former forbidden band while two new transmission troughs arise at 1326 nm and 1470 nm, respectively. The magnetic field responses for all the peaks and troughs are provided in Fig. 1(c), which show the details of SPPs propagations and distributions in the MIM waveguide structures. The phase shifts versus the wavelength of the SRR and DRR systems are plotted in Fig. 1(d). Obviously, a $\pi$-phase shift arises at the induced transparency window for the DRR system. Usually, the dispersion $d_\rho$ and the time delay $\tau$ satisfy the condition $d_\rho = d\tau/d\lambda$, where $\tau$ is determined by the phase slop $2\pi\partial\theta/\partial f$. In this case, the normal dispersion occurs in the transparent window, and thus, the enhanced group delay is obtained. This characteristic may be beneficial to the applications of slow light and data storage. Besides, the PIT transmission spectrum is quite sensitivity to refractive index $n$ of the surrounded material [34], [35]. On the basis of the DRR system in Fig. 1(b), the refractive index of the dielectric is changed to be $n = 1.1$. Obviously, the transmission spectrum has a large red shift by increasing $n$ from 1.0 to 1.1, as shown in Fig. 2. The increasing range of wavelengths for the two transmission toughs are 131.9 nm and 145.0 nm, respectively. Therefore, we can obtain the large sensitivities from the variations of the two toughs as 1319 nm/RIU and 1450 nm/RIU, respectively. As such, it is considered that the structure may be used as a nano sensor.

To find out more characteristics of the DRR system, we arrange an inclined angle $\theta$ for RR2, as shown in Fig. 3. In the following, $\theta$ is used to denote the position of RR2, i.e. the case of $\theta = 0^\circ$ is the same as that of Fig. 1(b). When SPPs are captured into RR1, there are two different coupling pathways from the left side and right side of RR1 to RR2. We can consider there will be two different resonance modes that will interact with the mode in RR2, respectively, and this mechanism may lead to two PIT peaks. By setting $\theta = 30^\circ$, $r_2 = 122$ nm, $R_2 = 180$ nm, and keeping the other parameters unchanged, we can obtain the transmission spectrum with red solid line in Fig. 4(a) based on FDTD method. To evaluate the performances, the transmission spectrum of the DRR with $\theta = 0^\circ$ is still plotted by a blue dotted line, and by comparison, we can see that additional transmission peak (with transmittance of ~0.8) arises at the former left

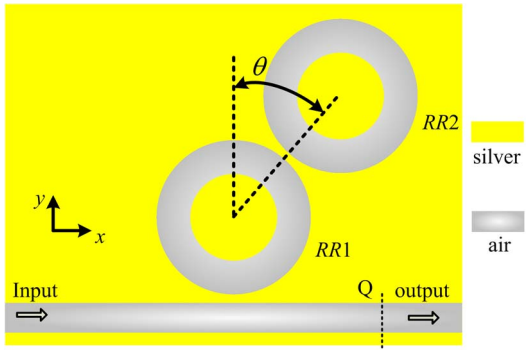


Fig. 3. MIM waveguide DRR system with an inclined angle $\theta$.

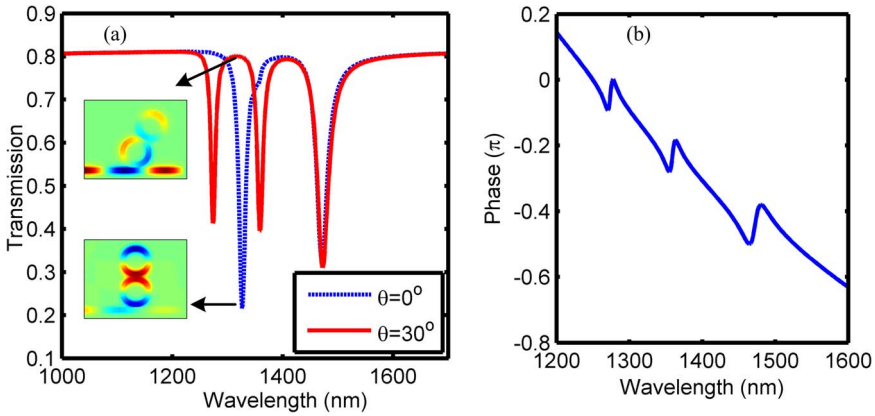


Fig. 4. (a) Transmission spectra of DRR system with $\theta = 0°$, 30°, and (b) phase shift of DRR system with $\theta = 30°$.

transmission trough (with transmittance of ~0.2 around 1326 nm). More details can be found in the magnetic field distribution of Fig. 4(a). SPPs at the peak wavelength can pass through the MIM bus waveguide, but the ones at the trough wavelength will be stopped by the ring resonator. Meanwhile, the former center transmission peak and right transmission trough remain unchanged, i.e. the transmittances for the peak and the right trough are ~0.8 and ~0.3, and they still stay at the former wavelengths. Since two transmission peaks are obtained, we consider that second order PIT effect is achieved. To get insight into phase condition at the wavelength ranges of two transparency windows, the phase shift is provided in Fig. 4(b). Similar to the result in Fig. 1(d), normal dispersion is available in the two transparency windows. This characteristic may offer the convenience for multi-channel slow light applications.

In the following, the transmission spectra are studied by changing the inclined angle $\theta$ and the coupling distance $d$, respectively. In Fig. 5(a), the angle $\theta$ is defined as 15°, 30°, and 45°, while other parameters are the same as that in Fig. 4(a). It can be seen that dual transparency peaks with high transmittance are almost available. The left and the center transmission troughs stay at the original wavelength but the right troughs, which are at 1484 nm, 1470 nm, and 1528 nm, respectively, are changed slightly. Besides, the transmission spectra are shown in Fig. 5(b) by setting $d = 5$ nm, 10 nm, 15 nm, and $\theta = 30°$. In this case, the wavelengths of the right transmission trough, which are 1470 nm, 1420 nm, and 1395 nm, respectively, have significantly blue shift, leading to the gradually disappearance of the right transparency window, as shown in Fig. 5(b). This phenomenon may be attributed to coupling effect that is weakened by increasing the coupling distance.

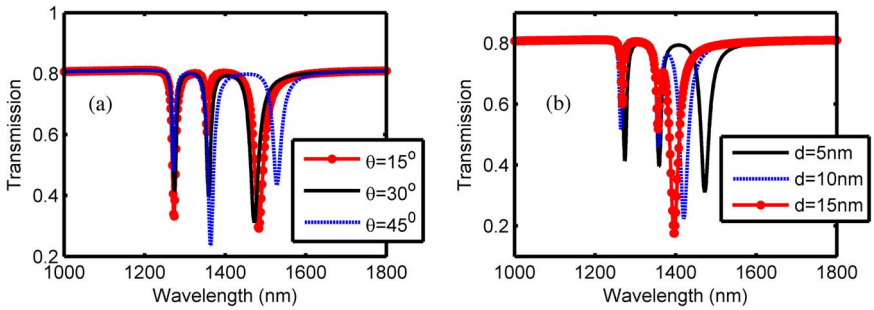


Fig. 5. Transmission spectra with (a) different inclined angle $\theta$ and (b) different coupling distance $d$.

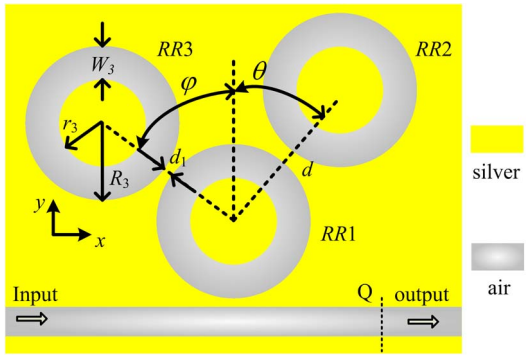


Fig. 6. MIM waveguide TRR system.

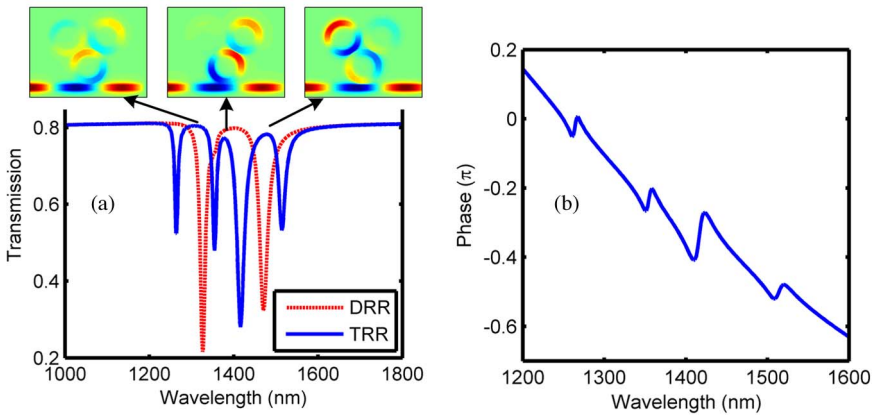


Fig. 7. (a) Transmission spectra of TRR system with $\varphi = 35^\circ$ and (b) phase shift of TRR system.

According to the results and analysis, it is known that dual transparency windows are achieved in Fig. 4(a) by using the DRR system with $\theta = 30^\circ$. Actually, the right transmission trough in Fig. 4(a) can also be eliminated through the third-order PIT effect, which can be achieved by adding the third RR on the basis of the DRR system. Fig. 6 shows the triple RR (TRR) system where RR3 is placed on another side of RR1 with an inclined angle $\varphi$ and a coupling distance $d_1$. In addition to the interference effect between RR1 and RR2, extra destructive interference will also occur between RR1 and RR3. By appropriately defining the parameters, the third transparency window will arise. In the following simulations, we define the inner and out radiuses as $r_3 = 137$ nm and $R_3 = 180$ nm, respectively, the coupling distance as $d_1 = 5$ nm, and the inclined angle as $\varphi = 35^\circ$, while other parameters are the same as that used in Fig. 4.

The simulated transmission spectra and the magnetic field distributions for the peaks are shown in Fig. 7(a). Comparing the results in Fig. 4(a), an extra transmission peak is obtained at the wavelength of 1470 nm which is also the transmission trough for the DRR system. Obviously, three transparency windows with high transmittances of ~0.8 are obtained in the proposed MIM waveguide TRR system. The magnetic field distributions demonstrate that SPPs at the three peak wavelengths can propagate through the MIM waveguide, and thus the PIT phenomena are well investigated from another aspect. The phase shifts with respect to the wavelength are shown in Fig. 7(b). Obviously, phase shifts will emerge along with each transparency peak, and thus, steep linear normal dispersions for three windows can be used to compensate the signal for each channel without large significant attenuation.

## 3. Conclusion

The wavelength selection performance for the MIM waveguide SRR system has been investigated. Then, PIT phenomenon was obtained by using a DRR system, since a transparency window arose at the wavelength of the former band gap. Furthermore, DRR and TRR structures with inclined angles have been proposed and investigated. Multi-level PIT effects have been obtained due to the additional higher order destructive interference effects between the ring resonators. Based on the FDTD simulation method, dual and triple transparency windows with high transmittances of ~0.8 have been achieved at the wavelengths of 1326 nm, 1373 nm, and 1470 nm, respectively. These structures could find wide applications in the photonic integration fields of sensitive sensor, optical data storage, etc.

## References


[1] M. Fleischhauer, A. Imamoglu, and J. P. Marangos, "Electromagnetically induced transparency: Optics in coherent media," *Rev. Mod. Phys.*, vol. 77, no. 2, pp. 633–673, Jul. 2005.

[2] R. W. Boyd and D. J. Gauthier, "Photonics: Transparency on an optical chip," *Nature*, vol. 441, no. 7094, pp. 701–702, Jun. 2006.

[3] S. Zhang, D. A. Genov, Y. Wang, M. Liu, and X. Zhang, "Plasmon-induced transparency in metamaterials," *Phys. Rev. Lett.*, vol. 101, no. 4, Jul. 2008, Art. ID 047401.

[4] N. Liu *et al.,* "Planar metamaterial analogue of electromagnetically induced transparency for plasmonic sensing," *Nano Lett.*, vol. 10, no. 4, pp. 1103–1107, Apr. 2010.

[5] R. D. Kekatpure, E. S. Barnard, W. Cai, and M. L. Brongersma, "Phase-coupled plasmon induced transparency," *Phys. Rev. Lett.*, vol. 104, no. 24, Jun. 2010, Art. ID 243902.

[6] D. D. Smith, H. Chang, K. A. Fuller, A. T. Rosenberger, and R. W. Boyd, "Coupled resonator induced transparency," *Phys. Rev. A, At., Mol., Opt. Phys.*, vol. 69, no. 9, Jun. 2004, Art. ID 063804.

[7] Q. Xu *et al.,* "Experimental realization of an on-chip all-optical analogue to electromagnetically induced transparency," *Phys. Rev. Lett.*, vol. 96, no. 12, Mar. 2006, Art. ID 123901.

[8] X. G. Luo and L. S. Yan, "Surface plasmon polaritons and its applications," *IEEE Photon. J.*, vol. 4, no. 2, pp. 590–595, Apr. 2012.

[9] M. B. Pu *et al.,* "Investigation of Fano resonance in planar metamaterial with perturbed periodicity," *Opt. Exp.*, vol. 21, no. 1, pp. 992–1001, Jan. 2013.

[10] M. B. Pu *et al.,* "Catenary optics for achromatic generation of perfect optical angular momentum," *Sci. Adv.*, vol. 1, no. 9, Oct. 2015, Art. ID e1500396.

[11] F. F. Hu, H. X. Yi, and Z. P. Zhou, "Wavelength demultiplexing structure based on arrayed plasmonic slot cavities," *Opt. Lett.*, vol. 36, no. 8, pp. 1500–1502, Apr. 2011.

[12] J. Chen *et al.,* "Coupled-resonator-induced Fano resonances for plasmonic sensing with ultra-high figure of merits," *Plasmonics*, vol. 8, no. 4, pp. 1627–1631, Dec. 2013.

[13] H. Lu, X. Liu, D. Mao, and G. Wang, "Plasmonic nanosensor based on Fano resonance in waveguide-coupled resonators," *Opt. Lett.*, vol. 37, no. 18, pp. 3780–3782, Sep. 2012.

[14] K. H. Wen *et al.,* "Fano resonance with ultra-high figure of merits based on plasmonic metal-insulator-metal waveguide," *Plasmonics*, vol. 10, no. 1, pp. 27–32, Feb. 2015.

[15] K. H. Wen *et al.,* "Design of an optical power and wavelength splitter based on subwavelength waveguides," *J. Lightw. Technol.*, vol. 32, no. 17, pp. 3020–3026, Sep. 2014.

[16] X. Luo *et al.,* "Plasmonic filter using metal–insulator–metal waveguide with phase shifts and its transmission characteristics," *Plasmonics*, vol. 9, no. 4, pp. 887–892, Aug. 2014.

[17] X. J. Shang *et al.,* "Realizing Fano-like resonance in a one terminal closed T-shaped waveguide," *Eur. Phys. J. B*, vol. 88, no. 6, p. 144, Jun. 2015.

[18] Y. Matsuzaki, T. Okamoto, M. Haraguchi, M. Fukui, and M. Nakagaki, "Characteristics of gap plasmon waveguide with stub structures," *Opt. Exp.*, vol. 16, no. 21, pp. 16314–16325, Oct. 2008.

[19] A. R. Halpern and R. M. Corn, "Lithographically patterned electrodeposition of gold, silver, and nickel nanoring arrays with widely tunable near-infrared plasmonic resonances," *ACS Nano*, vol. 7, no. 2, pp. 1755–1762, Feb. 2013.
[20] D. Lehr *et al.,* "Plasmonic properties of aluminum nanorings generated by double patterning," *Opt. Lett.*, vol. 37, no. 2, pp. 157–159, Jan. 2012.
[21] M. Bayati, P. Patoka, M. Giersig, and E. Savinova, "An approach to fabrication of metal nanoring arrays," *Langmuir*, vol. 26, no. 5, pp. 3549–3554, Mar. 2010.
[22] Y. Cai, Y. Li, P. Nordlander, and P. Cremer, "Fabrication of elliptical nanorings with highly tunable and multiple plasmonic resonances," *Nano Lett.*, vol. 12, no. 9, pp. 4881–4888, Sep. 2012.
[23] G. Cao *et al.,* "Plasmon-induced transparency in a single multimode stub resonator," *Opt. Exp.*, vol. 22, no. 21, pp. 25215–25223, Oct. 2014.
[24] Y. Huang, C. Min, and G. Veronis, "Subwavelength slow-light waveguides based on a plasmonic analogue of electromagnetically induced transparency," *Appl. Phys. Lett.*, vol. 99, no. 14, Oct. 2011, Art. ID 143–117.
[25] G. Wang, H. Lu, and X. Liu, "Dispersionless slow light in MIM waveguide based on a plasmonic analogue of electromagnetically induced transparency," *Opt. Exp.*, vol. 20, no. 19, pp. 20902–20907, Sep. 2012.
[26] G. Cao *et al.,* "Formation and evolution mechanisms of plasmon-induced transparency in MDM waveguide with two stub resonators," *Opt. Exp.*, vol. 21, no. 8, pp. 9198–9205, Apr. 2013.
[27] Z. Chen and L. Yu, "Multiple Fano resonances based on different waveguide modes in a symmetry breaking plasmonic system," *IEEE Photon. J.*, vol. 6, no. 6, Dec. 2014, Art. ID 4802208.
[28] H. Lu, X. M. Liu, D. Mao, Y. K. Gong, and G. X. Wang, "Induced transparency in nanoscale plasmonic resonator systems," *Opt. Lett.*, vol. 36, no. 16, pp. 3233–3235, Aug. 2011.
[29] Z. H. Han and S. I. Bozhevolnyi, "Plasmon-induced transparency with detuned ultracompact Fabry–Perot resonators in integrated plasmonic devices," *Opt. Exp.*, vol. 19, no. 4, pp. 3251–3257, Feb. 2011.
[30] B. Huang *et al.,* "Plasmonic-induced transparency and slow-light effect based on stub waveguide with nanodisk resonator," *Plasmonics*. 2015, DOI:10.1007/s11468-015-0085-1.
[31] Z. Chen *et al.,* "Spectral splitting based on electromagnetically induced transparency in plasmonic waveguide resonator system," *Plasmonics*, vol. 10, no. 3, pp. 721–727, Jun. 2014.
[32] K. H. Wen *et al.,* "Electromagnetically induced transparency-like transmission in a compact side-coupled T-shaped resonator," *J. Lightw. Technol.*, vol. 32, no. 9, pp. 1701–1707, May 2014.
[33] J. A. Dionne, L. A. Sweatlock, and H. A. Atwater, "Plasmon slot waveguides: Towards chip-scale propagation with subwavelength-scale localization," *Phys. Rev. B, Condens. Matter Mater. Phys.*, vol. 73, no. 3, Jan. 2006, Art. ID 035407.
[34] Z. Chen *et al.,* "Tunable electromagnetically induced transparency in plasmonic system and its application in nanosensor and spectral splitting," *IEEE Photon. J.*, vol. 7, no. 6, Dec. 2015, Art. ID 4801408.
[35] B. X. Li *et al.,* "High sensitivity sensing based on plasmon induced transparency," *IEEE Photon. J.*, vol. 7, no. 5, Oct. 2015, Art. ID 4801207.